

Slack Dynamics on an Unfurling String

J. A. Hanna* and C. D. Santangelo†

Department of Physics, University of Massachusetts, Amherst, MA 01003

(Dated: May 11, 2022)

We consider the phenomenon of a noisy arch growing on a rapidly deployed thin object contacting a rigid plane. We present a qualitative model for the growing structure involving the amplification, rectification, and advection of slack in the presence of a quasi-steady stress field, validate our assumptions with numerical experiments, and pose new questions about the spatially developing motions of thin objects.

arXiv:1202.0795v1 [cond-mat.soft] 3 Feb 2012

* hanna@physics.umass.edu

† csantang@physics.umass.edu

The deployment of a thin object from a roll or pile is a canonical event, important for textile manufacture [1–3], tethered satellite control [4–6], and successful use of anchor rodes, drogues, watch chains, and garden hoses. Despite this ubiquity, we were recently surprised by an observation of these dynamics, as embodied by a rapidly straightened chain on a tabletop [7]. The surprise in question is displayed in Figure 1. One free end of an orderly monolayer of chain is rapidly pulled along a table, leading to the formation of a slowly growing, wobbling, noisy arch near the pick-up point. The phenomenon is not unique to chains, and may be observed in strings or ropes [8] and other quasi-one-dimensional objects. We will use the words “chain” and “string” interchangeably in what follows. This letter details some results that arise from consideration of the simplest possible system resembling that of Figure 1, which we believe shed some light on the phenomenon of the arch.

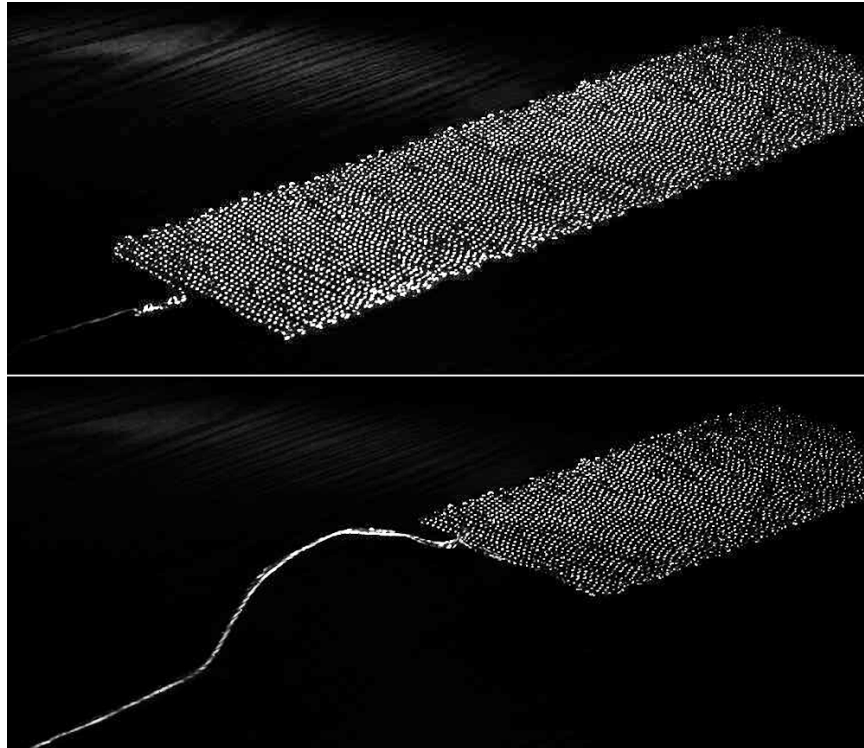


FIG. 1. Still images from a video [7] showing configurations of a chain tightly woven on a table before (top) and during (bottom) a straightening process. A vertically-oriented arch is apparent in the latter image. Chain links are ~ 2 mm, the amplitude of the initial condition is ~ 5 cm, the imposed velocity of the pulled end is ~ 8 m/s.

Given a time-dependent curve $\mathbf{X}(s, t)$ parametrized by arc length s , the wave equation

$$\mu \partial_t^2 \mathbf{X} = \partial_s (\sigma \partial_s \mathbf{X}) \quad (1)$$

describes a balance of inertia and line tension in a string of uniform mass density μ . The stress $\sigma(s, t)$, morally equivalent to the pressure in a one-dimensional fluid, is a multiplier field enforcing the metrical constraint $\partial_s \mathbf{X} \cdot \partial_s \mathbf{X} = 1$ [9–18]. This equation is in principle derivable as the zero-radius limit of an elastic rod, the continuum limit of a chain of rigid links or, more abstractly, from a Lagrangian living on a curve. Taking an arc length derivative of (1) and projecting along the unit tangent $\partial_s \mathbf{X}$ yields the auxiliary equation

$$\partial_s^2 \sigma - \sigma \kappa^2 = -\mu \partial_t \partial_s \mathbf{X} \cdot \partial_t \partial_s \mathbf{X}, \quad (2)$$

the solution of which serves to impose the constraint [9, 13–18]. The “screening potential” of this Poisson-like equation is the squared curvature $\kappa^2 = \partial_s^2 \mathbf{X} \cdot \partial_s^2 \mathbf{X}$, while the “source term” on the right hand side has been rewritten in terms of the magnitude of the rate of change of the unit tangent using $\partial_t \partial_s \mathbf{X} \cdot \partial_s \mathbf{X} = 0$. From this form, it appears that the stresses induced by inertial motions of the string will be tensile unless one imposes unfavorable boundary or initial conditions. Positivity of the stress is proven for one fixed and one free end [18] and the proof may be extended [19]. Hence, we will not generally be concerned with unstable evanescent dynamics that might arise from imaginary wave speeds in (1).

Relevant to our problem are a class of solutions to (1) and (2) for which the curve motion is purely tangential, $\partial_t \mathbf{X} = T \partial_s \mathbf{X}$. Here, \mathbf{X} is arbitrary and T and $\sigma = \mu T^2$ are uniform along the curve [20]. The shape \mathbf{X} itself is simply one of two solutions, namely that which travels at speed $-T$ with respect to the Lagrangian frame of (1) moving at speed T along the curve. It is thus stationary in the laboratory frame; this and the linear dispersion inherent when σ is uniform are used to great effect in certain kinetic sculptures [21, 22].

The addition of a uniform gravitational term $\mu \mathbf{g}$ to the right hand side of (1) breaks the degeneracy in \mathbf{X} and may generate compressive stresses. The remaining stationary-shape solutions of this augmented equation are the catenaries [17, 23] with the tangential velocity T determining the tension, not the shape. Given that compression ($\sigma < 0$) corresponds to catastrophic failure, we can naively assume inertial stabilization of a symmetric catenary arch $\kappa = \frac{a}{a^2 s^2 + 1}$, a a negative constant, bearing a tension $\sigma = \mu \left(T^2 + \|\mathbf{g}\| \frac{\sqrt{a^2 s^2 + 1}}{a} \right)$, as long as the length parameters of the shape fall within a circle whose radius is the natural length scale defined by the velocity and gravity: $(\frac{1}{a})^2 + s^2 \leq \left(\frac{T^2}{\|\mathbf{g}\|} \right)^2$. At this point it is worth recalling the scales involved in Figure 1. The terminal “free stream” tangential velocity $T \sim 8$ m/s, \mathbf{g} is Earth gravity (~ 10 m/s²), and $\kappa \geq \sim 10$ /m for the duration of the experiment. Hence, the ratio of inertial to gravitational accelerations $\frac{T^2 \kappa}{\|\mathbf{g}\|}$ is at least on the order of fifty to a hundred. So gravity is neglectable here, due to the large curvature that spontaneously emerges early in the process. The natural time scale of about one second ($\frac{T}{\|\mathbf{g}\|}$) is equally irrelevant. Adding a rigid motion with comparable velocity to the analysis—a wobbling perpendicular to the catenary’s plane, for example—does not change the order of magnitude of the relevant terms. However, given sufficient growth time, or a stiffer curve with a bending or twisting length scale that could set a lower bound on this initial emergent curvature, gravity may come into play. We will also neglect drag on the chain by air and table.

Returning to our original equations (1) and (2), let’s consider an initially planar curve \mathbf{X} with a small perturbation $\delta b \hat{\mathbf{b}}$ oriented perpendicular to the osculating planes of \mathbf{X} , in this case simply the plane containing \mathbf{X} . To first order in the perturbation, we have the decoupled equations

$$\mu \partial_t^2 \delta b = \partial_s (\sigma \partial_s \delta b), \quad (3)$$

$$\partial_s^2 \delta \sigma - \delta \sigma \kappa^2 = 0, \quad (4)$$

such that $\delta \sigma = 0$, and the height function δb moves through a stress background determined entirely by the planar dynamics. Modulo the periodic component of the motion induced by the initial chain layout, material particles take heteroclinic trajectories between two arbitrary stationary shapes with tangential velocities of zero in the pile and the imposed pulling velocity downstream. Although we might expect velocity and stress discontinuities at the moving front, we may also clearly observe a smooth transition region for the velocity [7], which presumably corresponds to a smooth transition in stress. The dynamics as a whole appear to be nearly steady; even the arch grows slowly and remains within a nearly constant distance from the front. Thus, with an imposed pulling velocity T , we introduce the traveling wave variable $\eta \equiv s + Tt$, presume some $\sigma(\eta)$, and approximate the slowly evolving dynamics (3) with the equation

$$\partial_\eta \left[\partial_t \delta b = \frac{\sigma(\eta) - \mu T^2}{2\mu T} \partial_\eta \delta b \right]. \quad (5)$$

This is a short-time description of $b(\eta, t)$ that presumes smallness of second order time derivatives, in a frame Eulerian with respect to the curve but not the laboratory. It admits general solutions, for which the characteristics converge at infinite time, of the form $\delta b = f \left(t + \int^\eta d\eta' \frac{2\mu T}{\sigma(\eta') - \mu T^2} \right)$, f an arbitrary function. Figure 2 compares the evolution of a wave packet under (3) and the integrated form of (5) for a tanh-shaped $\sigma(\eta)$ that interpolates between zero and the free stream stress μT^2 . Agreement is good for early times, when the packet is “squeezed” behind the free stream. The disturbance eventually reaches a nearly stationary configuration *via* a complicated modulated motion, not captured by the first order transport equation (5). Note that the area under the height function does not represent any “energy-like quantity to be conserved” [17] in this transport equation, so that in this approximation, squeezing the packet does not increase its amplitude.

The initial squeezing is best expressed in a new variable, the “slack” $l \equiv \sqrt{(\partial_s \delta b)^2}$ taken up into the height function. In terms of l , the transient dynamics (5) take the form

$$\partial_t l = \partial_\eta \left(\frac{\sigma(\eta) - \mu T^2}{2\mu T} l \right). \quad (6)$$

Given a monotonically increasing $\sigma(\eta)$, (6) is comprised of an amplification and an advection term. These are the ingredients for a convectively unstable system [24–27]. However, in contrast to the open flow systems usually

considered in this context, both the amplification and advection coefficients in (6) drop to zero as the material particle moves downstream through a stress field that smoothly approaches its free stream value. The slack pools behind the free stream, as shown in the lower inset of Figure 2. This should correspond to a location near the upstream base of the arch.

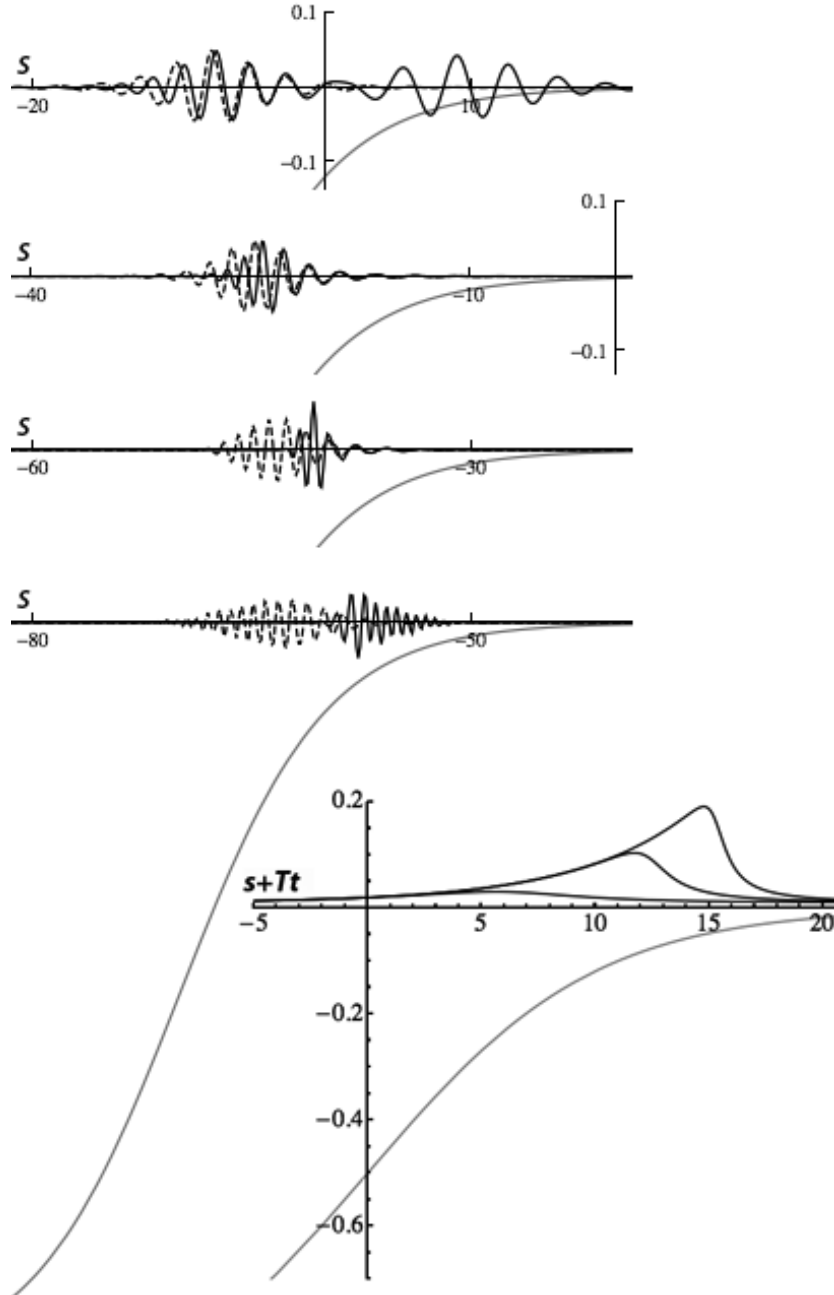


FIG. 2. The grey curves are all $\frac{\sigma}{\mu T^2} - 1$, where $\sigma = \frac{\mu T^2}{2} [1 + \tanh(\frac{\eta}{10})]$ and $\eta \equiv s + Tt$. TOP AND CENTER: The evolution of a wave packet $\delta b(s, t)$ under (3) (full black lines) and the integrated form of (5) (dashed black lines), for $\mu = T = 1$, at times $t = 10, 30, 50, 70$, as viewed in a frame Eulerian on the string, with the downstream direction to the right and the horizontal axes representing s . The initial conditions at $\eta = s$ are $\delta b = 2b_0$ for (3) and $\delta b = b_0$ for (5), where $b_0 \equiv \frac{1}{20} \text{sech}(\frac{3\eta}{10}) \cos(2\eta)$. LOWER RIGHT INSET: The evolution of the slack variable $l \equiv \sqrt{(\partial_s \delta b)^2}$ under (6) (full black lines) for $\mu = T = 1$, at times $t = 50, 150, 250$, as viewed in a frame Eulerian on the string, with the downstream direction to the right and the horizontal axis representing $\eta \equiv s + Tt$. The initial condition at $\eta = s$ is uniform: $l = \frac{1}{100}$.

We have been talking about derivatives of the height rather than the height itself. However, in Figure 1, our slope amplifier is coupled to a height rectifier, namely a table. Is this sufficient for the formation of a structure? To

answer this, we have implemented a simple Verlet integration [28] of massive beads and stiff springs. This allows us to nullify bending and twist elasticity, frictional interactions with the table, and any other messy and experimentally unavoidable physics. The 5000 beads begin sinusoidally woven in a plane defined by the potential minimum created by a constant gravitational force perpendicular to a hard plane “table”, an exponential with argument 100 at a penetration depth of one spring rest length. A velocity perpendicular to the weave is imposed on one end bead. A small quantity of uniform noise is added to the vertical force on each bead at all times, and a damping coefficient of a few percent is introduced during the first few timesteps to counteract errors in specifying initial bead positions.

The snapshot of shape, stress, and height in Figure 3 is the result of a simulation with initial layout amplitude and frequency of ~ 6 cm and ~ 0.6 cycles/cm, parameters similar to Figure 1. We have set $\mu = \|\mathbf{g}\| = T = 1$, and the half-width of the uniform noise distribution is 10^{-3} . The extensions of the springs are used as a proxy for stress, and these data are spatially averaged. An initial attenuating pulse travels down the chain, leaving a nearly quiescent wake, followed by a rapid transition to the free-stream stress μT^2 . This very noisy stress plateau also carries oscillations due to the undamped lateral motions of the chain arising from its initial configuration. An arch does indeed form, on the downstream side of the transition. The effect of gravity in the simulation is rather minimal, affecting only the qualitative shape of the arch. Without the “table”, however, the slack isn’t rectified, and no arch forms. We also note that the dynamics are quite robust with respect to changes in the spring constant. The simulations shown in this letter involve strains of about 2.5% in the plateau, but the important features are quite similar for strains an order of magnitude larger or smaller. However, stiffer springs result in proportionally larger oscillatory stresses with respect to the plateau stress.

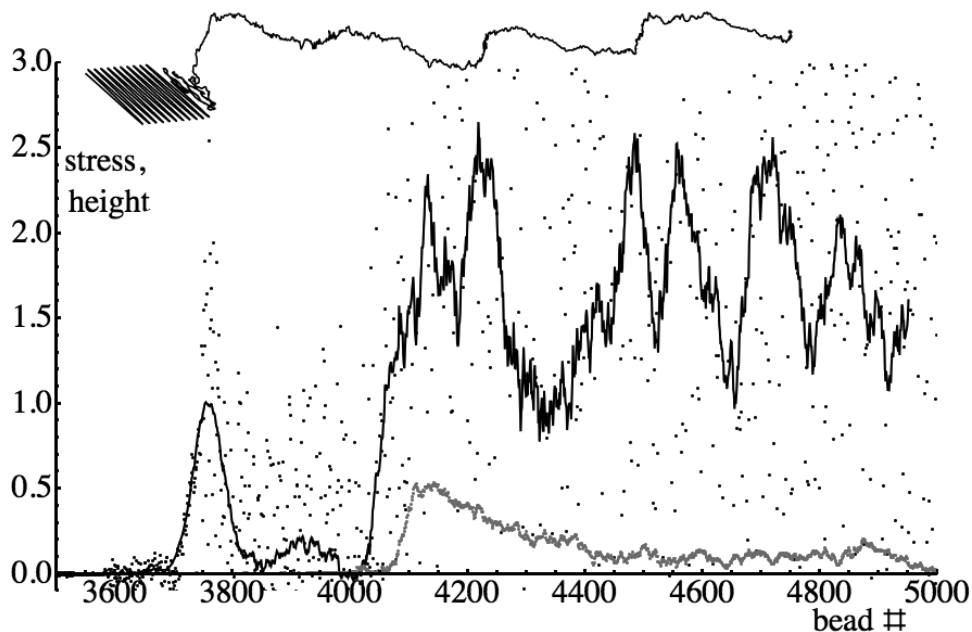


FIG. 3. Height (grey line, normalized by the initial layout amplitude), stress (black dots), and averaged stress (black line, moving average over 50 beads, normalized by the theoretical free stream stress $\mu T^2 = 1$) after 150 ms for a configuration with initial layout amplitude and frequency of ~ 6 cm and ~ 0.6 cycles/cm. The velocity boundary condition is imposed on bead #5000. A portion of the corresponding three-dimensional shape is shown in an oblique view in the upper left inset. Spring rest lengths are 2 mm, and the strain corresponding to a stress of 1 is 2.5%. The raw stress data extend from approximately -9 to +11 in the noisy plateau region. Noise from a uniform distribution of half-width 10^{-3} is added to vertical forces; this may be compared to $\mu\|\mathbf{g}\| = 1$ and spring forces on the order of 10^7 .

We return to our assumption of a steady stress distribution in the traveling wave frame. Figures 4 and 5 show snapshots of two chains at three identical times. The chain of Figure 4 is that of Figure 3, while that of Figure 5 corresponds to an initial arrangement with similar amplitude but lower frequency, ~ 6 cm and ~ 0.1 cycles/cm, and the same level of added noise. The high-frequency chain appears to sustain a steady, or perhaps very slowly growing, transition region between low and high velocity, and is highly receptive to noise. This region moves approximately 6-7 beads/ms upstream, not much faster than the traveling wave coordinate (5 beads/ms). The transition region on the low-frequency chain steadily widens as the chain unfurls, its leading edge moving significantly faster upstream (9-11 beads/ms), and out-of-plane growth is slower to develop and less pronounced. Over the time interval shown, this region retains much qualitative information about its initial shape even as the material within it has achieved

highly tangential velocities. The stress on this chain appears to reflect this ordered arrangement, although the nature of the pulse train in Figure 5 remains to be explored.

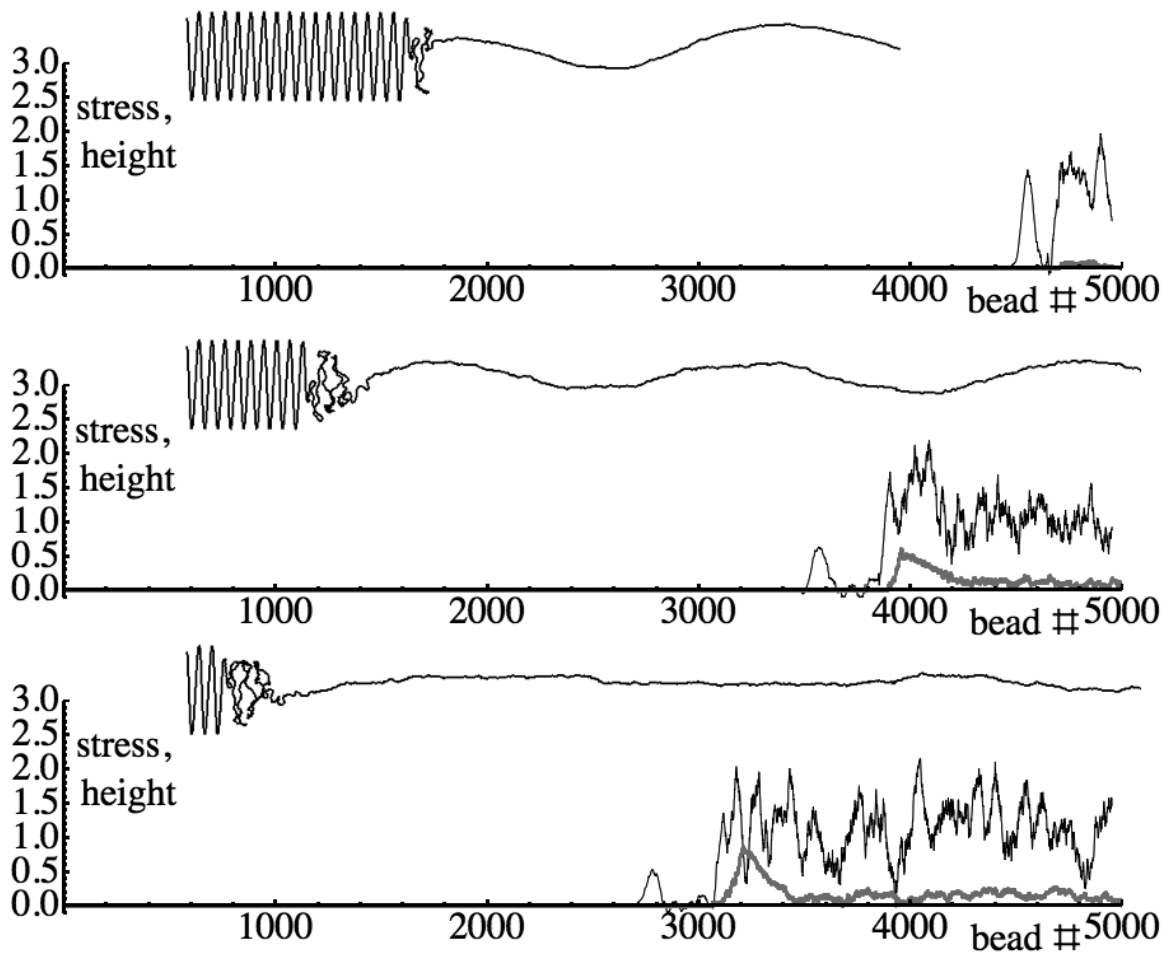


FIG. 4. Height (grey lines, normalized by the initial layout amplitude) and averaged stress (black lines, moving average over 50 beads, normalized by the theoretical free stream stress $\mu T^2 = 1$) after 55, 175, and 295 ms for a configuration with initial layout amplitude and frequency of ~ 6 cm and ~ 0.6 cycles/cm. Top views of a portion of the corresponding shapes are shown in the upper insets. Other details as for Figure 3.

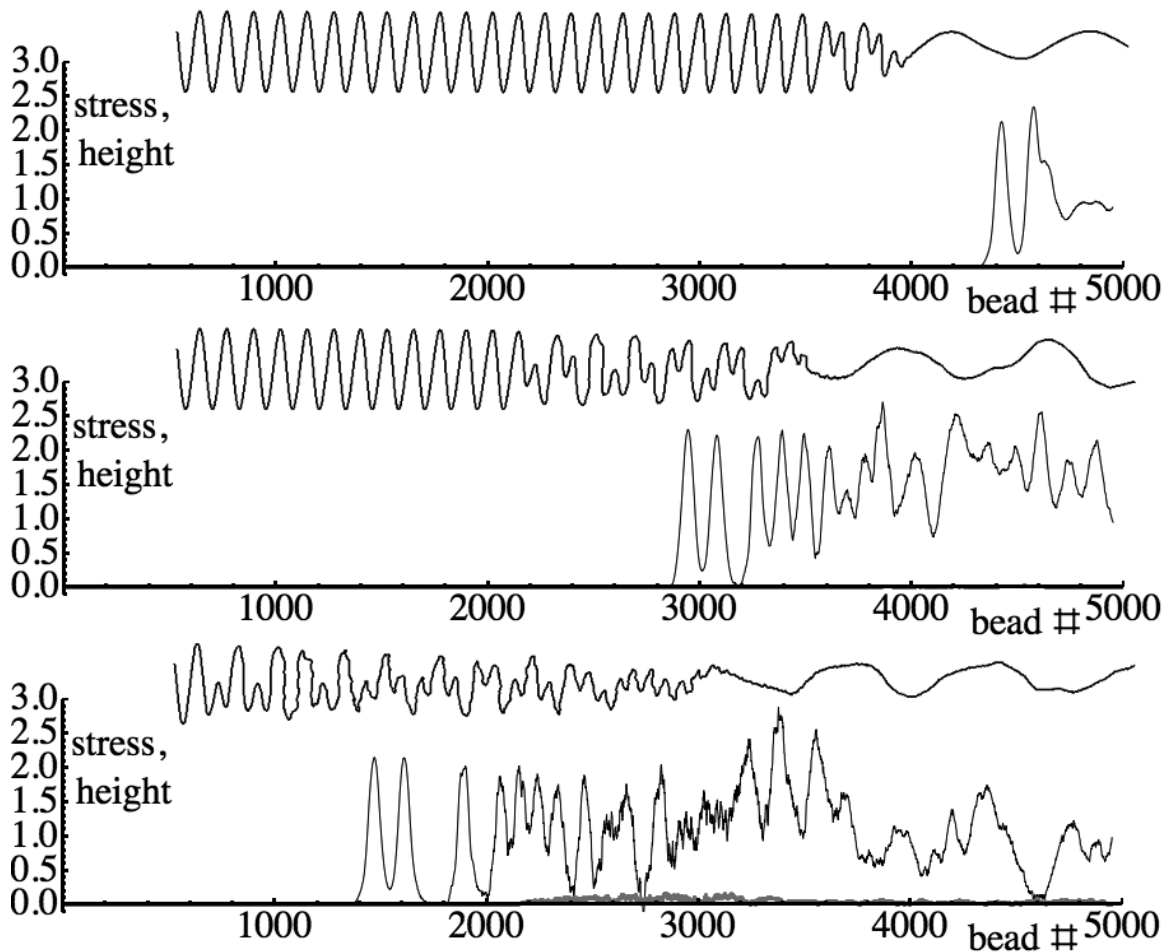


FIG. 5. Height (grey lines, normalized by the initial layout amplitude) and averaged stress (black lines, moving average over 50 beads, normalized by the theoretical free stream stress $\mu T^2 = 1$) after 55, 175, and 295 ms for a configuration with initial layout amplitude and frequency of ~ 6 cm and ~ 0.1 cycles/cm. Top views of a portion of the corresponding shapes are shown in the upper insets. Other details as for Figure 3.

In Figure 6, we show the maximum height of the high-frequency configuration of Figures 3 and 4, with levels of added noise between 10^{-3} and 10^{-15} . There is a clear trend towards an earlier appearance of the arch with higher noise levels, but even roundoff errors will generate nontrivial effects.

Our preliminary study has raised several questions. Perhaps most interesting is the issue of how to analyze the planar dynamics we see in the insets of Figures 4 and 5, and the associated stress generation, in terms of the time-dependent screening and source terms of equation (2). There is some sort of signal being transmitted along our string, conveying information about the velocity boundary condition. The process of transmission is highly dependent on the evolving shape of the curve, and thus more complicated than transverse impulsive loading of a straight string [29]. Interesting physics arises from gradients in the stress, which are absent in the Klein-Gordon-type equations describing the perturbative dynamics around stationary states of elastic rods [30], though we note that a uniform but time-varying tension is known to cause instabilities of planar motions of fixed-end strings [31]. What slowly evolving stress distributions can be sustained by moving elastic curves? And which spatially developing motions will inevitably bear noisy structures like our arch? Are there analogues in elastic sheets, nets, fluid membranes, or the Navier-Stokes equations in certain geometries? Incompressibility of the system appears merely an analytical convenience, not a strict requirement. Finally, we have disregarded the periodic aspects of the curve's motion, and still lack an explicit description of the role of the rectifying potential. Is it possible to describe the arch growth as a secular result of some forcing by the table, perhaps on the high-curvature turning points of the curve, or is the resemblance to a resonance superficial?

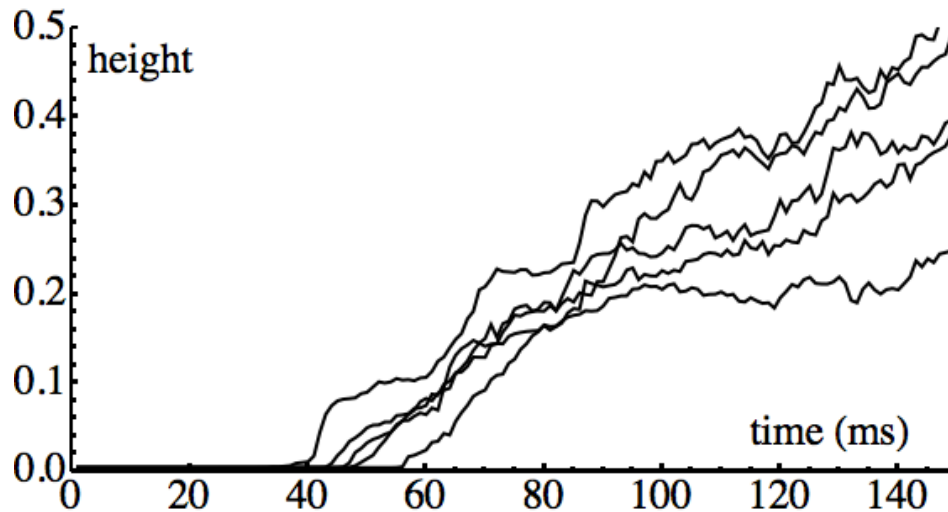


FIG. 6. Maximum height (normalized by the initial layout amplitude) as a function of time for a configuration with initial layout amplitude and frequency of ~ 6 cm and ~ 0.6 cycles/cm, with noise added to vertical forces from uniform distributions of half-widths (from left to right or top to bottom) 10^{-3} , 10^{-6} , 10^{-9} , 10^{-12} , and 10^{-15} . Each curve is an average of three runs; take-off times of individual curves are highly reproducible. The lowest noise level is indistinguishable from roundoff noise up to a time of about 60-65 ms. Normalized spring rest lengths are ~ 0.033 .

ACKNOWLEDGMENTS

We thank H. King and N. Menon for assistance and encouragement, and J. Machta for a discussion. JAH thanks B. Mbanga for advice on simulations, R. Schroll for a two-timing tutorial, P. Kevrekidis for a discussion, and B. Eckhardt for a suggestion about frames. Funding came from National Science Foundation grant DMR 0846582.

-
- [1] D. G. Padfield. The motion and tension of an unwinding thread. I. *Proc. R. Soc. Lond. A*, 245:382–407, 1958.
 - [2] V. K. Kothari and G. A. V. Leaf. The unwinding of yarns from packages. Part I: The theory of yarn unwinding. Part II: Unwinding from cylindrical packages. *J. Text. Inst.*, 70:89–104, 1979.
 - [3] W. B. Fraser, T. K. Ghosh, and S. K. Batra. On unwinding yarn from a cylindrical package. *Proc. R. Soc. Lond. A*, 436:479–498, 1992.
 - [4] V. V. Beletsky and E. M. Levin. *Dynamics of Space Tether Systems*. American Astronautical Society, San Diego, 1993.
 - [5] K. K. Mankala and S. K. Agrawal. Dynamic modeling and simulation of satellite tethered systems. *J. Vib. Acoust.*, 127:144–156, 2005.
 - [6] M. Krupa, W. Poth, M. Schagerl, A. Steindl, W. Steiner, H. Troger, and G. Wiedermann. Modelling, dynamics and control of tethered satellite systems. *Nonlinear Dynamics*, 43:73–96, 2006.
 - [7] J. A. Hanna and H. King. An instability in a straightening chain. [arXiv:1110.2360], 2011.
 - [8] A. Savage and J. Hyneman. Tablecloth chaos. <http://www.imdb.com/title/tt1747319/>, 2010.
 - [9] S. F. Edwards and A. G. Goodyear. The dynamics of a polymer molecule. *J. Phys. A: Gen. Phys.*, 5:965–980, 1972.
 - [10] M. Reeken. The equation of motion of a chain. *Math. Z.*, 155:219–237, 1977.
 - [11] T. J. Healey. Stability and bifurcation of rotating nonlinearly elastic loops. *Q. Appl. Math.*, 48(4):679–698, 1990.
 - [12] E. J. Hinch. Brownian motion with stiff bonds and rigid constraints. *J. Fluid Mech.*, 271:219–234, 1994.
 - [13] R. E. Goldstein and S. A. Langer. Nonlinear dynamics of stiff polymers. *Phys. Rev. Lett.*, 75(6):1096–1097, 1995.
 - [14] A. Thess, O. Zikanov, and A. Nepomnyashchy. Finite-time singularity in the vortex dynamics of a string. *Phys. Rev. E*, 59(3):3637–3640, 1999.
 - [15] M. J. Shelley and T. Ueda. The Stokesian hydrodynamics of flexing, stretching filaments. *Physica D*, 146:221–245, 2000.
 - [16] A. Belmonte, M. J. Shelley, S. T. Eldakar, and C. H. Wiggins. Dynamic patterns and self-knotting of a driven hanging chain. *Phys. Rev. Lett.*, 87(11):114301, 2001.
 - [17] M. Schagerl and A. Berger. Propagation of small waves in inextensible strings. *Wave Motion*, 35:339–353, 2002.
 - [18] S. C. Preston. The motion of whips and chains. [arXiv:1105.1944], 2011.
 - [19] S. C. Preston. personal communication, 2012.
 - [20] T. J. Healey and J. N. Papadopoulos. Steady axial motions of strings. *J. Appl. Mech.*, 57:785–787, 1990.
 - [21] J. Aitken. Experiments illustrating rigidity produced by centrifugal force. *Proc. Phil. Soc. Glas.*, 9:99–106, 1876.

- [22] N. Tuck. Lariat chain. <http://www.normantuck.com/catalogPages/lariat.html>, 1986.
- [23] N. C. Perkins and C. D. Mote, Jr. Three-dimensional vibration of travelling elastic cables. *J. Sound Vib.*, 114(2):325–340, 1987.
- [24] R. J. Deissler. Noise-sustained structure, intermittency, and the Ginzburg-Landau equation. *J. Stat. Phys.*, 40(3/4):371–395, 1985.
- [25] R. J. Deissler and J. D. Farmer. Deterministic noise amplifiers. *Physica D*, 55:155–165, 1992.
- [26] P. Huerre and P. A. Monkewitz. Local and global instabilities in spatially developing flows. *Annu. Rev. Fluid Mech.*, 22:473–537, 1990.
- [27] J.-M. Chomaz. Global instabilities in spatially developing flows: Non-normality and nonlinearity. *Annu. Rev. Fluid Mech.*, 37:357–392, 2005.
- [28] D. Frenkel and B. Smit. *Understanding Molecular Simulation*. Academic Press, San Diego, 1996.
- [29] M. F. Beatty and J. B. Haddow. Transverse impact of a hyperelastic stretched string. *J. Appl. Mech.*, 52:137–143, 1985.
- [30] A. Goriely and M. Tabor. Nonlinear dynamics of filaments II. Nonlinear analysis. *Physica D*, 105:45–61, 1997.
- [31] C. Gough. The nonlinear free vibration of a damped elastic string. *J. Acoust. Soc. Am.*, 75(6):1770–1776, 1984.